Understanding the vibrational spectra of crystalline isoniazid: Raman, IR and INS spectroscopy and solid-state DFT study

Paulo J.A. Ribeiro-Claro, Pedro D. Vaz, Mariela M. Nolasco, Ana M. Amado

PII:	S1386-1425(18)30615-2
DOI:	doi:10.1016/j.saa.2018.06.073
Reference:	SAA 16232
To appear in:	*Spectrochimica Acta Part A: Molecular and Biomolecular Spectroscopy*
Received date:	2 April 2018
Revised date:	13 June 2018
Accepted date:	20 June 2018

Please cite this article as: Paulo J.A. Ribeiro-Claro, Pedro D. Vaz, Mariela M. Nolasco, Ana M. Amado , Understanding the vibrational spectra of crystalline isoniazid: Raman, IR and INS spectroscopy and solid-state DFT study. Saa (2018), doi:10.1016/j.saa.2018.06.073

Understanding the Vibrational Spectra of Crystalline Isoniazid: Raman, IR and INS Spectroscopy and Solid-State DFT Study

Paulo J. A. Ribeiro-Claro[a], Pedro D. Vaz[b,c], Mariela M. Nolasco[a] and Ana M. Amado*,[d]

[a] CICECO, Departamento de Química, Universidade de Aveiro, P-3810-193 Aveiro, Portugal.

[b] ISIS Neutron & Muon Source, Rutherford Appleton Laboratory, Chilton, Didcot, Oxfordshire OX11 0QX, UK

[c] CQB, Departamento de Química e Bioquímica, Faculdade de Ciências da Universidade de Lisboa, 1749-016 Lisboa, Portugal.

[d] Química-Física Molecular, Departamento de Química, FCTUC, Universidade de Coimbra, P-3004-535 Coimbra, Portugal.

‡ Corresponding author:
email: amado.am@gmail.com
Telf. +351-234 370732

Abstract

This work presents a comprehensive spectroscopic analysis of crystalline isoniazid, one of the main drugs in tuberculosis chemotherapy, using a blend of spectroscopic and computational methods. Mid- and far-infrared, Raman, and inelastic neutron scattering spectroscopies, with contribution of isotopic substitution are combined with discrete and periodic DFT quantum chemical calculations. This combined approach successfully reproduces the whole spectral range, allowing a sound assignment of all the vibrational bands. Previous misassignments have been corrected and several spectral features of isoniazid crystal are reported for the first time. Virtues and limitations of the computational approach (periodic and discrete) are also discussed in light of the present state-of-the-art in the field.

Keywords:; Quantum chemical calculations; Periodic calculations; CASTEP; Vibrational assignments; Hydrogen bonding

1. INTRODUCTION

Vibrational spectroscopy is being increasingly used and recognized as a relevant tool in pharmaceutical research technology, namely, in the characterization and monitoring of pharmaceutically active ingredients and pharmaceutical formulations **[1-7]**. Applications include chemical structure elucidation, routine chemical analysis and solid-state characterization, embracing polymorphism, hydration/dehydration, crystallinity, and co-crystal formation **[3, 5, 7-11].** Both Raman and infrared spectroscopy have been extensively exploited to generate process analytical technologies (PAT) used for routine process control in pharmaceutical manufacturing and bioprocessing **[5, 7]**

The assignment of the vibrational spectra evolved from the empirical approach based on the comparison of similar molecules to the current "computational spectroscopy" *era* **[12]**. The computational description of molecular solids has been approached using discrete calculations of molecular associations (e.g., **[13, 14]**), but periodic methods – available through programs such as VASP **[15]**, CRYSTAL **[16]** and CASTEP **[17]** – are becoming increasingly popular. The rising application of the periodic density functional theory calculations in the study of pharmaceutically important systems can be evidenced from a few recent publications **[18-23]**.

Nevertheless, the plane wave/pseudopotential approach is still presenting problems in the description of specific vibrational modes **[19-21, 24-27]** and discrete calculations are often used complementarily, due to their well-known consistency and reliability.

Isoniazid (pyridine-4-carbohydrazide, also known as isonicotinic acid hydrazide (scheme 1) is still one of the main drugs used in tuberculosis chemotherapy. Moreover, being a GRAS molecule (Generally Regarded As Safe), with ability to form molecular associations with carboxylic acid bearing molecules **[28]**, it is also particularly interesting in the expanding field of pharmaceutical co-crystals.

[Scheme]

Isoniazid provides a clear example of the current status concerning the elucidation of the vibrational spectra of pharmaceutically active ingredients. Early assignments of isoniazid are frequently partial and often conflicting in several relevant points **[29-32]**. The more recent quantum chemical calculations **[30-38]** fail to select the most stable conformational form of the molecule or the correct hydrogen-bond contacts present in the crystal, leading to ill-based vibrational assignments. This situation precludes the full use of vibrational spectroscopy in the study of isoniazid systems and justifies a more comprehensive work.

The present work performs a complete vibrational analysis (Raman, mid- and far-Infrared, and Inelastic Neutron Scattering (INS) spectroscopies) on crystalline isoniazid. INS spectroscopy is a vibrational spectroscopic technique which provides information not amenable from its optical counterparts (IR and Raman). In short, in INS there are no selection rules for the activity of vibrational modes, and the signal intensity is proportional to nuclei displacement and to incoherent neutron scattering cross-section of the nuclei, both of which are particularly high for hydrogen atoms. Molecular characterization of the drug is complemented with discrete and periodic quantum chemical calculations, using DFT methods, as they have proven to be a valuable auxiliary tool in the analysis and interpretation of experimental vibrational spectra.

2. EXPERIMENTAL AND THEORETICAL DESCRIPTION

2.1 Sample preparation

Crystalline samples of title compound were prepared by dissolving 1.5 g (10.9 mmol) of isoniazid (Sigma-Aldrich, CAS: 54-85-3) in 5 mL of distilled water at 40ºC and allowing the solution to slowly cool to ambient conditions and left to stand overnight. The resulting white elongated prismatic crystals were removed from the solution, put under a continuous flow of dry air for 1 night, and stored in sealed vials. N-deuterated samples, isoniazid-*d3* (ca. 96% D), were obtained similarly, using D_2O as solvent.

2.2 Vibrational spectroscopy

FT-Raman spectra: Room-temperature Fourier Transform Raman (FT-Raman) spectra were recorded on an RFS-100 Bruker FT spectrometer, using an Nd:YAG laser with an excitation wavelength of 1064 nm. Each spectrum is the average of three repeated measurements of 150 scans each with a resolution of 2 cm^{-1}.

ATR-FTIR spectra: The ATR-FTIR spectra were measured on a Vertex 70 spectrometer using a Platinum ATR single reflection diamond accessory. For the far-IR spectrum (50-600 cm^{-1}) a silicon solid-state beamsplitter and a Deuterated L-alanine doped TriGlycine Sulphate (DLaTGS) detector with a polyethylene window was used. The mid-IR spectrum (400-4000 cm^{-1}) was recorded using a Ge on KBr substrate beamsplitter and a liquid nitrogen cooled wide band Mercury Cadmium Telluride (MCT) detector. All spectra are the average of two counts of 128 scans each. A spectral resolution of 2 cm^{-1} was used. In order to minimize the Christiansen effect, the sample was mixed with KBr powder.

INS spectra: Inelastic neutron scattering experiment was performed with the TOSCA spectrometer, an indirect geometry time-of-flight spectrometer at the ISIS Neutron and Muon Source at the Rutherford Appleton Laboratory (Chilton, UK). The sample, with a total amount of 2 g, was packed inside flat thin-walled aluminum can of 5 cm height and 4 cm width, with a path length of 2 mm, which were then mounted perpendicular to the beam using a regular TOSCA centre-stick. Spectra were collected below 10 K and measured for 180 micro-amps (μA) of proton current.

2.3 Theoretical calculations

Periodic density functional theory (periodic-DFT) calculations were carried out using the plane-wave/pseudopotential method as implemented in the CASTEP code **[16, 39]**. Exchange and correlation were approximated using the PBE **[40]** functional. The plane-wave cut-off energy was 830 eV. Brillouin zone sampling of electronic states was performed on 8 × 4 × 4 Monkhorst-Pack grid.

The equilibrium structure, an essential prerequisite for lattice dynamics calculations was obtained by LBFGS geometry optimization of reported crystal structure (CSD entry: INICAC02) **[28]**, after which the residual forces were converged to zero within 0.005 $eV \cdot A^{-1}$. In a first step, the experimental cell parameters were kept constant during “constant volume” geometry optimization. In

a second step, the cell parameters were relaxed and a full geometry optimization was performed.

Phonon frequencies at the Gamma point were obtained by diagonalization of dynamical matrices computed using density-functional perturbation theory **[41]**. The atomic displacements in each mode that are part of the CASTEP output, enable visualization of the modes to aid assignments and are also all that is required to generate the INS spectrum using the program aClimax **[42]**. It is emphasized that for all the calculated spectra shown the transition energies were not scaled and include wings and overtones up to 0-10 transitions, as implemented in aClimax **[42]**.

In order to evaluate the effects of intermolecular interactions in the vibrational spectra, and to assist the normal mode assignment, discrete calculations were performed using the Gaussian 09w program version (G09w) **[43]** using the mPW1PW91 DFT combined with the widely used 6-31G* basis set as defined in the Gaussian program **[43]**. The mPW1PW91/6-31G* level was considered as it has been found to yield a good compromise between accuracy and computational costs **[44-46]**.

All geometries were fully optimized within the Berny algorithm, using redundant internal coordinates, and considering the programs default convergence criteria **[43]**. Vibrational frequency calculations (including estimation of the Raman activities) were performed for all optimized geometries, at the same theory level, in order to verify convergence to a real minimum (no negative eigenvalues), to infer the magnitude of energetic corrections (*e.g.*, zero-point vibrational (zpve) and thermal) and to help in vibrational mode description. To assist in the identification of the vibrational modes directly associated to the amine groups, additional frequency calculations were performed for the NH– and NH_2–deuterated forms of isoniazid (*freq=ReadIsotopes* keyword **[43]**). In order to compare with the experimental wavenumbers, all calculated vibrational frequency were corrected for anharmonicity and incomplete electron correlation treatment using scaling factors reported in the literature for mPW1PW91/6-31G* level: 0.9828 and 0.9499 for the frequencies predicted, respectively, below and above 500 cm^{-1} **[47]**.

Estimation of the effects of the intermolecular interactions on the magnitude of the predicted vibrational frequencies was done using a pairwise approach which circumvents the high computational cost of using a molecular cluster to model the

crystal and is fully described elsewhere **[13].** In short, vibrational frequencies of the isolated molecule are corrected using the vibrational shifts predicted for molecular pairs that describe the distinct interactions present in the crystal structure. This approach has proven to be a useful tool in the assignment and interpretation of the vibrational spectrum of different supramolecular systems **[9, 10, 13, 14, 46, 48, 49]**.

NBO calculations **[50]** were performed in order to infer the bond order index of the intermolecular interactions holding the dimer structures.

Visualization of the atomic displacements characterizing each vibrational mode was performed using the Jmol program **[5]**.

3. RESULTS AND DISCUSSION

3.1 Molecular geometry and intermolecular interactions

Figure 1 illustrates the optimized geometries of the isolated molecule (discrete calculations, Gaussian09) and of the crystalline structure (periodic calculations, CASTEP) of isoniazid. For the isolated molecule, the values of torsional angles at the mPW1PW91/6-31G* level are shown.

[FIGURE 1]

The fragment of the optimized structure of crystalline isoniazid (Figure 1, right) is used to illustrate the relevant intermolecular contacts within the crystal. At the scale shown, there is no significant distinction between calculated and x-ray structures **[28]**. The isoniazid crystal structure is held by a network of N–H···N and C–H···O intermolecular interactions and Figure 1 depicts the participation of each isoniazid molecule as hydrogen bond donor. The representative molecule (identified with an arrow) presents two strong hydrogen bonds (N2H···N3, N3H···N1) and two weaker C-H···O contacts. Of course, the same molecule is the hydrogen-bond acceptor of equivalent contacts from other neighbouring molecules. For the sake of clarity, the molecules involved in π···π stacking with the reference molecule are not represented. All together, these interactions lead to the formation of an infinite spiral-type crystal structure, as fully described in the literature **[28, 51, 52]**. The above contacts have been the basis to build the four molecular pairs used in discrete calculations (see Fig. 3S, Suppl. Mat.).

Table 1 presents some selected geometrical parameters of the carbohydrazide fragment of isoniazid, obtained from discrete mPW1PW91/6-31G* and periodic PBE calculations and x-ray crystallography. Both discrete and periodic results are in good agreement with the experimental values, yielding RMS deviations for bond lengths and bond angles in the order of 1%.

[TABLE 1]

Two points deserve discussion, regarding periodic and discrete results, respectively. Periodic calculations with full optimization result in an increase of cell dimensions, which is residual in the “b” and “c” directions, but rather large in the “a” direction. As it can be seen from Table 1, this large increment of “a” axis size affects all geometrical parameters, but it is clearly related to the increase of π stacking distance (as measured from the distance between C1 atoms of staked molecules). On the other hand, discrete calculations show that the minimum energy conformation in the crystal is not a minimum for the isolated molecule. In fact, the orientation of the carbohydrazide group relative to the aromatic ring plane is not correctly described by Gaussian calculations. This is easily visualized considering the N–H bond nearly perpendicular to the plane of the aromatic ring, which will be hereafter labelled as “axial NH”. For both X-ray and CASTEP structures, with all $\theta_{1\text{-}3}$ angles negative, the axial NH (NHb) and the oxygen atom are in opposite sides of the ring plane. In the isolated molecule, the θ_2 angle is positive and, as a result, the axial NH (NHa) and the oxygen atom lie in the same side of the ring plane.

Needless to say, the quality of calculated frequencies used to assist the assignment of vibrational spectra is highly dependent on the correctness of the input model, in what concerns molecular geometry and intermolecular interactions (see, for instance, **[45, 46, 53-55]**). However, a few recent quantum chemical calculations fail to select the most stable conformational form of the molecule **[30, 34, 36, 37]** or the correct hydrogen-bond contacts in the x-ray structure **[31, 32, 34, 35, 38]**, and this confines the reliability of the reported vibrational assignments. Concerning the isoniazid isolated molecules, Favilla *et al.* **[30]** refer a planar geometry, with the NH_2 group being slightly deviated from planarity, while several authors selected the *anti* configuration of the carbohydrazide group ($\theta_2 \approx 180^o$) for the global energy minimum

[30, 31, 34, 36-38] instead of the *syn* configuration ($\theta_2 \approx -6^o$) observed experimentally. Some quantum chemical calculations **[32, 34, 35]** also used dimeric isoniazid structures to explain the effects of the hydrogen bonds of the crystal on the vibrational frequencies. However, most of the dimeric structures assembled do not mimic any intermolecular interactions that actually occur in the isoniazid crystalline structure. For instance, dimeric structures held by N–H···O hydrogen bonds and centrosymmetric NH···N dimers are considered **[32, 34, 35]** although such interactions are not observed in the crystalline structure.

3.2 The Vibrational spectra

The isoniazid crystal is orthorhombic, with space group symmetry $P2_12_12_1$ and Z=4, presenting 68 atoms in the crystallographic unit cell (17 atoms per isolated molecule), from which 201 optical modes are predicted. These include 180 normal vibration modes of the four molecules ($45A+45B_1+45B_2+45B_3$) and 21 external modes describing translations and rotations (9 translational modes plus 12 librational modes, $6A+5B_1+5B_2+5B_3$).

Considering the 45 normal modes of vibration of each individual molecule, 27 are related to the pyridine ring and the remaining to the carbohydrazide fragment. The ring-related modes can be described as 11 stretching modes (4x νCC, 2x νCN, 4x νCH and νC1–R; R=substituent), 8 in-plane deformation modes (3x αring, 4x βCH and βC1–R) and 8 out-of-plane deformation modes (3 δring, 4 γCH and γC1–R). The 18 modes related to the carbohydrazide group, on the other hand, can be described as 6 stretching modes (νC=O, νC6–N2, νN2–N3, 2x $\nu N3H_2$, νN2H), 4 in-plane deformation modes (βC=O, $\beta C1$–C6–N2, βN2H and βC6–N2–N3), 2 out-of-plane deformation modes (γC=O and γN2H), 3 $N3H_2$-related deformation modes (scissoring, twisting and wagging) and 3 torsional modes (τC1–R, τC6–N2 and $\tau N2–N3H_2$).

Table 2 lists the observed bands in each spectroscopy and their assignments, in accordance with the modes itemized above. The calculated CASTEP values refer to the fully optimized structure. The comparison between wavenumber values

obtained from “fixed cell” and “fully optimized” structures reveals that cell optimization leads to a general decrease of the calculated frequencies, with a notable exception for the CH stretching modes and some modes around the 500 cm^{-1} region (See Fig 1S , Suppl. Mat). However, this does not yield a significant change in the agreement with the experimental frequencies, since the average deviation (calculated-experimental) is ca. 2% for both cases (See Fig 2S , Suppl. Mat).

[TABLE 2]

The assignments in Table 2 are made in terms of “approximate description” of the normal modes – referring to the most relevant contribution to each normal mode. This approach is assumed to be a more practical, although less rigorous, alternative to the description based on the potential energy distribution (PED). Nevertheless, the coupling between oscillators is more a rule than an exception, and several modes present substantial mixing despite their simple description on Table 2. Two relevant examples are shown in Fig. 2. The mode at 804 cm^{-1} is the expected in-phase out-of-plane bend of the four CH bonds, but has a significant participation of the out-of-plane bending of the NH bond lying nearly in the same plane (N2H). The mode at 1190 cm^{-1} is ascribed to the N2–N3 stretch, but displays important contribution from C1–C6 stretch, although the νC1–C6 mode is better assigned to the band at 1320 cm^{-1}.

[FIGURE 2]

The high wavenumber region: CH and NH stretching modes

The assignment of the vibrational modes of isoniazid in the region of the NH and CH stretching modes is not a trivial task, mainly due to strong mechanical and electrical anharmonicity affecting the hydrogen-bonding N–H oscillators. The INS spectrum (Fig. 3a), despite its low resolution in this region, clearly identifies the 2950-3350 cm^{-1} interval for the “H-moving” vibrations. The Raman spectrum (Fig. 3b) confirms the CH stretching modes in the 3065 cm^{-1} vicinity, while the infrared

spectrum (ATR, Fig. 3c) reveals a typical anharmonic profile due to the presence of strong NH···N hydrogen bonds: a broad absorption band, spanning from nearly 2400 cm^{-1} up to 3300 cm^{-1}, presenting several maxima. This profile has been ascribed to several effects (vibrational couplings between high- and low-frequency stretching modes in hydrogen bonds, resonance interactions among different hydrogen bonds in the unit cell, Fermi resonance between the fundamental stretching and the overtone of the in-plane bending vibrations **[56]** and electrical anharmonicity **[57, 58]**). Whatever its origin, its complexity precludes a straightforward assignment of the normal modes. This is achieved, however, with the complementary information provided by isotopic substitution (Fig. 3d) and periodic frequency calculations (Fig. 3e), as discussed below.

[Figure 3]

The assignment of the four νCH modes becomes straightforward from the comparison between the experimental spectrum of the N-deuterated sample and the calculated spectrum (Fig. 3, d and e). The corresponding Raman bands are easily identified therefrom.

On the other hand, the assignments of the three νNH modes deserve more discussion. It has been reported that periodic calculations underestimate the stretching frequencies of hydrogen-bonded OH **[21, 25]** and NH groups **[27]**. Nevertheless, periodic calculations clearly identify the band at *ca.* 3304 cm^{-1} with the vibration of the $N3H_a$ bond in the terminal amino group (Fig.3, c and e). This particular vibrational mode results from the fact that $N3H_a$ bond is isolated, in the sense that both N2H and $N3H_b$ are involved in much stronger hydrogen bonding and combine between them. This is a result from periodic calculations that cannot be predicted by discrete calculations with monomer or dimers. Upon deuteration, the $\nu N3H_a$ band moves to *ca.* 2457 cm^{-1}, as easily identified in Fig.3d. The observed isotopic ratio νNH/νND is 1.35, while the value obtained for the diatomic harmonic N–H oscillator is 1.37.

CASTEP periodic calculations predict the remaining two νNH modes of the N2HN3H$_2$ fragment (described as $\nu_{sym}N_2H_2$ and $\nu_{as}N_2H_2$) to arise below 3000 cm^{-1}, with very large intensity. The location of νNH modes below the νCH ones is assumed to be an error of the method, as mentioned above. Most probably, the νN_2H_2 modes contribute to the Raman/ATR band at *ca.* 3108/3105 cm^{-1} and to the INS intensity above this wavenumber. On the other hand, comparison between the spectra of normal and N-deuterated samples (Fig. 2 c and d) clearly shows that these modes are responsible for the whole profile in the infrared spectrum. Both calculations and isotopic substitution agree that the contribution of νCH intensities to the infrared profile is negligible when compared with the $\nu N3H_2$ contributions.

Previous reports do not consider the coupling between the νN2H and νN3Hb oscillators (with isolation of νN3Ha) that results from intermolecular hydrogen-bonding. Pandey et al. **[31]** and Gunasekaran et al. **[36]** ascribe the Raman band at around 3300 cm^{-1} to the νN2H (isolated) mode. Gobinath et al. **[38]**, on the other hand, assign the bands at *ca.* 3300, 3110 and 3430 cm^{-1} in the conventional way (asymmetric and symmetric combinations of the $\nu N3H_2$, and νN2H, respectively).

The mid wavenumber region: completing molecular modes

In the 200-1750 cm^{-1} region, the calculated spectra provide a very good description of the experimental INS and infrared spectra (Fig. 4 and 5, respectively). Apart the notable exceptions of the bands indicated with dashed arrows, there is a nearly one-to-one match between calculated and observed intensities. The visual match is better in the INS case than in the infrared case, as the latter is affected by anharmonicity effects (in addition, the Christiansen effect produce derivative-like line shapes). Nevertheless, the combined analysis of both spectra allows a sound assignment of the normal modes in this region.

[Figure 4]

[Figure 5]

In this region, the ill-calculated vibrational modes (dashed arrows) are the carbonyl stretching mode and the $–NH_2$ torsion mode. It has been observed previously that CASTEP-PBE calculations underestimate the frequency of C=O stretching mode **[19, 20, 24, 26]** and the possible source of this effect has been discussed **[20, 24]**. On the other hand, the above mentioned problems for the N–H stretching modes also embrace bending and torsion modes within the $NH–NH_2$ fragment (similar problems with NH_2/NH_3 groups can be observed in the work of Pawlukojc *et al*. **[19]** for the L-Glutamine molecular crystal). Nevertheless, this vibrational modes are easily assigned by comparing relative band intensities.

In contrast with the assignment described in Table 2, previous assignments are often incomplete, inconsistent with isotopic substitution data and generally conflicting. An illustrative case is the assignment of the C=O stretching and NH_2 scissoring modes, at 1661 and 1632 cm^{-1}, respectively (FTIR). Considering the most recent publications **[31, 32, 36, 38]**, only the assignment of Owen et al. **[32]** agrees with ours. There is no reference to the NH_2 mode in the work of Gunaserekan et al. **[36]**, while Gobinath et al. **[38]** assign it to a band at 1602 cm^{-1}. More recently, Pandey et al. **[31]** swap the order of νC=O and NH_2 scissoring modes, ascribing a higher wavenumber band to the NH_2 mode (1635 cm-1, FTIR) and a lower wavenumber band to the νC=O mode (1556 cm^{-1}, FTIR). The N2–H “in-plane” bending mode, βNH, also deserves clarification. In some reports no reference is made to this mode **[31, 36]**, while others ascribe it to a Raman band observed at 1154 cm^{-1} **[38]** or to bands observed at 1130 (IR) and 1335 cm^{-1} (FT-Raman) **[32]**. The βNH vibrational mode has been referred as highly coupled to the νC(6) –N(2) stretching mode, giving rise to two bands, one around 1550 cm^{-1} and one other at *ca*. 1135 cm^{-1} **[59]**. In the higher frequency mode, nitrogen and hydrogen atoms move in opposite directions **[59]**. This band is also more sensitive to deuteration than its lower wavenumber counterpart, and hence it is ascribed to the βNH mode.

Periodic calculations predict an observable splitting for βC=O, τC6–N2, βring–R, γring–R and τC1–C6 modes, as shown at the bottom rows of Table 2. Factor group splitting is inherently present, since there are four molecules in the orthorhombic cell (Z=4), and each molecular mode is expected to give rise to four crystal modes. For most of the vibrational modes the factor group components are

very close together - at least, within spectral resolution - and have limited influence in the observed spectra. However, for these large amplitude molecular vibrations, significant splitting is predicted and observed. This crystal effect has been neglected in previous assignments, despite its obvious presence in both infrared and Raman spectra.

The low wavenumber region: collective modes

The description of the low wavenumber region can only be obtained from periodic calculations, as this is the region of the external lattice modes, i.e., modes involving translation and rotation (libration) of the molecules.

Figure 6 compares the experimental spectra of isoniazid in the low-wavenumber region (INS and far-IR) with the PBE calculated spectra. As it can be seen, calculated spectra provide a poorer description of the low frequency modes. It has been recognized that numerical errors of periodic calculations tend to accumulate in this range **[21, 24]**. Nevertheless, there is a reasonable correspondence between the overall calculated and observed band profile, allowing a description of low frequency/large amplitude collective modes.

[Figure 6]

Low frequency collective modes are known to present significant mixing of intermolecular and intramolecular vibrations **[58, 60]** and that prevents their description in a simple form. Recently, several works attempted to depict these modes of molecular crystals using both text-descriptive **[18, 20, 21, 23]** and figure-illustrative approaches (*e.g.*, molecular projections with displacement arrows) **[18, 20-22]**. However, figures with displacement arrows are often cumbersome and only in limited cases a 2D projection denote the 3D motion. Description of modes can be more informative, providing there is a clear identification of the system axes. In Table 4, the modes are described in terms of translations along the crystallographic cell axes (a, b, c) and librations around the molecular inertia axes (Ia, Ib, Ic). The reason for the two sets of axes is that some collective motions are better described as “unit cell motions”, while others are molecule-centered motions. Nevertheless, the descriptions of the modes do not reflect their complex and coupled nature, rather

focusing on the most relevant contributions to each observed band. For instance, the motion of the whole molecule as nearly a rigid body (pure translational modes) can be ascribed to the INS band at *ca.* 37 cm^{-1} (translation along b axis). Libration motions at 47, 69, 101 and 118 cm^{-1} are clearly coupled with pyridine-carbohydrazide torsions.

[TABLE 3]

Table 3 also includes the identification of lattice modes with contribution from hydrogen bond stretching modes, namely, the N2H···N3 stretching (129 cm^{-1}) and the N3H···N1 stretching (110 cm^{-1}). Of course, in a crystal lattice, these modes are not pure νH···N modes, as they would be in an isolated dimer. However, they present a significant motion of the donor group towards/away the acceptor nitrogen atom along the hydrogen-bond direction, as illustrated in Fig. 7 for the higher frequency mode ν(N2H···N3). The relative frequencies of these modes follow the relative strength of the hydrogen bond contacts, as it can be inferred from the interatomic distances and NBO analysis. According to the x-ray structure (see Table 1) the N3···N2 distance is *ca.* 12 pm shorter than the N1···N3 distance, signaling a stronger hydrogen bond. NBO analysis confirms the same trend. The Wiberg bond orders for N3···H(N2) and N1···H(N3) are 0.0520 and 0.0378, respectively. Significantly, the lattice mode that presents a contribution from stretching of the much weaker CH···O contacts (with Wiberg bond orders below 0.003) is calculated at 80 cm^{-1}.

[Figure 7]

4. CONCLUSIONS

The vibrational properties of crystalline isoniazid have been fully described using a blend of spectroscopic techniques and computational methods. In combination with its optical counterparts (Raman and infrared spectroscopies), inelastic neutron scattering (INS) spectroscopy provides access to a detailed description of all the vibrational modes in the crystal. Periodic density functional

calculations using CASTEP were able to successfully reproduce the experimental spectra with a few exceptions. Discrete calculations are able to provide a better description of a few particular modes (e.g., carbonyl stretching and NH torsion modes), but only if the intermolecular interactions within the crystal are correctly taken into account.

This combined approach was able to successfully reproduce the whole spectral range, allowing a sound assignment of the vibrational bands. Previous misassignments have been corrected and several spectral features of isoniazid crystal - such as the unusual combination of NH oscillators in the NH stretching region, the factor group splitting observed for large amplitude molecular vibrations, and detailed description of lattice modes region - are reported for the first time. In this way, this study will hopefully contribute to further understand the structure of this API and to prevent the propagation of incorrect data analysis and misassignments.

The success in describing isoniazid vibrational spectra is particularly relevant in view of the urgent need of reliable computational approaches to elucidate the vibrational properties of molecular crystals – namely, due to the rising importance of vibrational spectroscopy as a tool in pharmaceutical research technology. The state-of-the-art solid-state density functional theory calculations (periodic boundary conditions, plane-wave DFT) gives deep insight into the vibrational properties of crystals and generally provides reliable assignment of the whole spectral range, except for a few well-identified and very specific modes, as discussed above.

ACKNOWLEDGMENTS

The authors acknowledge financial support from the Portuguese Foundation for Science and Technology – Unidade de Química-Física Molecular (UID/Multi/00070/2013) and project CICECO, Aveiro Institute of Materials, POCI-01-0145-FEDER-007679 (UID/CTM/50011/2013) – financed by national funds through the FCT/MEC and when appropriate co-financed by FEDER under the PT2020 Partnership Agreement. Acknowledgements are also due to the STFC

Rutherford Appleton Laboratory, in particular to Jeff Armstrong, for recording the INS spectrum. CASTEP calculations were made possible due to the computing resources provided by STFC Scientific Computing Department's SCARF cluster.
M. Nolasco also acknowledge FCT for the researcher contract under the program IF 2015, IF/01468/2015.

REFERENCES

[1] A. Heinz, C.J. Strachan, K.C. Gordon, T. Rades, Analysis of solid-state transformations of pharmaceutical compounds using vibrational spectroscopy, Journal of Pharmacy and Pharmacology, 61 (2009) 971-988.
[2] A. Chanda, A.M. Daly, D.A. Foley, M.A. LaPack, S. Mukherjee, J.D. Orr, G.L. Reid, D.R. Thompson, H.W. Ward, Industry Perspectives on Process Analytical Technology: Tools and Applications in API Development, Organic Process Research & Development, 19 (2015) 63-83.
[3] A. Erxleben, Application of Vibrational Spectroscopy to Study Solid- state Transformations of Pharmaceuticals, Current Pharmaceutical Design, 22 (2016) 4883-4911.
[4] E. Pindelska, A. Sokal, W. Kolodziejski, Pharmaceutical cocrystals, salts and polymorphs: Advanced characterization techniques, Advanced Drug Delivery Reviews, 117 (2017) 111-146.
[5] K.A. Esmonde-White, M. Cuellar, C. Uerpmann, B. Lenain, I.R. Lewis, Raman spectroscopy as a process analytical technology for pharmaceutical manufacturing and bioprocessing, Analytical and Bioanalytical Chemistry, 409 (2017) 637-649.
[6] D. Riolo, A. Piazza, C. Cottini, M. Serafini, E. Lutero, E. Cuoghi, L. Gasparini, D. Botturi, I.G. Marino, I. Aliatis, D. Bersani, P.P. Lottici, Raman spectroscopy as a PAT for pharmaceutical blending: Advantages and disadvantages, Journal of Pharmaceutical and Biomedical Analysis, 149 (2018) 329-334.
[7] N.L. Calvo, R.M. Maggio, T.S. Kaufman, Characterization of pharmaceutically relevant materials at the solid state employing chemometrics methods, Journal of Pharmaceutical and Biomedical Analysis, 147 (2018) 538-564.
[8] A.M. Amado, M.M. Nolasco, P.J.A. Ribeiro-Claro, Probing pseudopolymorphic transitions in pharmaceutical solids using Raman spectroscopy: Hydration and dehydration of theophylline, Journal of Pharmaceutical Sciences, 96 (2007) 1366-1379.
[9] M. Sardo, A.M. Amado, P.J.A. Ribeiro-Claro, Pseudopolymorphic transitions of niclosamide monitored by Raman spectroscopy, Journal of Raman Spectroscopy, 39 (2008) 1915-1924.
[10] M.M. Nolasco, A.M. Amado, P.J.A. Ribeiro-Claro, Effect of hydrogen bonding in the vibrational spectra of trans-cinnamic acid, Journal of Raman Spectroscopy, 40 (2009) 394-400.
[11] A.C. Jorgensen, C.J. Strachan, K.H. Pollanen, V. Koradia, F. Tian, J. Rantanen, An Insight into Water of Crystallization during Processing Using Vibrational Spectroscopy, Journal of Pharmaceutical Sciences, 98 (2009) 3903-3932.
[12] V. Barone, R. Improta, N. Rega, Quantum mechanical computations and spectroscopy: From small rigid molecules in the gas phase to large flexible molecules in solution, Accounts of Chemical Research, 41 (2008) 605-616.
[13] M.M. Nolasco, A.M. Amado, P.J.A. Ribeiro-Claro, Computationally-assisted approach to the vibrational spectra of molecular crystals: Study of hydrogen-bonding and pseudo-polymorphism, ChemPhysChem, 7 (2006) 2150-2161.
[14] M. Sardo, A.M. Amado, P.J.A. Ribeiro-Claro, Hydrogen bonding in nitrofurantoin polymorphs: a computation-assisted spectroscopic study, Journal of Raman Spectroscopy, 40 (2009) 1956-1965.
[15] G. Kresse, J. Furthmüller, Efficiency of ab-initio total energy calculations for metals and semiconductors using a plane-wave basis set, Computational Materials Science, 6 (1996) 15-50.
[16] R. Dovesi, R. Orlando, B. Civalleri, C. Roetti, V.R. Saunders, C.M. Zicovich-Wilson, CRYSTAL: a computational tool for the ab initio study of the electronic properties of crystals, Zeitschrift Für Kristallographie, 220 (2005) 571-573.
[17] S.J. Clark, M.D. Segall, C.J. Pickard, P.J. Hasnip, M.J. Probert, K. Refson, M.C. Payne, First principles methods using CASTEP, Zeitschrift Für Kristallographie, 220 (2005) 567-570.
[18] G.M. Day, J.A. Zeitler, W. Jones, T. Rades, P.F. Taday, Understanding the influence of polymorphism on phonon spectra: Lattice dynamics calculations and terahertz spectroscopy of carbamazepine, Journal of Physical Chemistry B, 110 (2006) 447-456.
[19] A. Pawlukojc, K. Holderna-Natkaniec, G. Bator, I. Natkaniec, L-glutamine: Dynamical properties investigation by means of INS, IR, RAMAN, H-1 NMR and DFT techniques, Chemical Physics, 443 (2014) 17-25.
[20] K. Druzbicki, J. Mielcarek, A. Kiwilsza, L. Toupet, E. Collet, A. Pajzderska, J. Wasicki, Computationally Assisted (Solid-State Density Functional Theory) Structural (X-ray) and Vibrational Spectroscopy (FT-IR, FT-RS, TDs-THz) Characterization of the Cardiovascular Drug Lacidipine, Crystal Growth & Design, 15 (2015) 2817-2830.
[21] K. Druzbicki, E. Mikuli, N. Palka, S. Zalewski, M.D. Ossowska-Chrusciel, Polymorphism of Resorcinol Explored by Complementary Vibrational Spectroscopy (FT-RS, THz-TDS, INS) and First-Principles Solid-State Computations (Plane-Wave DFT), Journal of Physical Chemistry B, 119 (2015) 1681-1695.

[22] P. Bilski, K. Druzbicki, J. Jenczyk, J. Mielcarek, J. Wasicki, Molecular and Vibrational Dynamics in the Cholesterol-Lowering Agent Lovastatin: Solid-State NMR, Inelastic Neutron Scattering, and Periodic DFT Study, Journal of Physical Chemistry B, 121 (2017) 2776-2787.
[23] L. Ding, W.H. Fan, X. Chen, Z.Y. Chen, C. Song, Terahertz spectroscopy and solid-state density functional theory calculations of structural isomers: Nicotinic acid, isonicotinic acid and 2-picolinic acid, Modern Physics Letters B, 31 (2017).
[24] K. Luczynska, K. Druzbicki, K. Lyczko, W. Starosta, Complementary optical and neutron vibrational spectroscopy study of bromanilic acid: 2,3,5,6-tetramethylpyrazine (1:1) cocrystal, Vibrational Spectroscopy, 75 (2014) 26-38.
[25] C.M. Lee, J.D. Kubicki, B.X. Fan, L.H. Zhong, M.C. Jarvis, S.H. Kim, Hydrogen-Bonding Network and OH Stretch Vibration of Cellulose: Comparison of Computational Modeling with Polarized IR and SFG Spectra, Journal of Physical Chemistry B, 119 (2015) 15138-15149.
[26] A. Pawlukojc, L. Hetmanczyk, INS, DFT and temperature dependent IR studies on dynamical properties of acetylcholine chloride, Vibrational Spectroscopy, 82 (2016) 37-43.
[27] S. Sahoo, T.R. Ravindran, S. Chandra, R.M. Sarguna, B.K. Das, T.N. Sairam, V. Sivasubramanian, C. Thirmal, P. Murugavel, Vibrational spectroscopic and computational studies on diisopropylammonium bromide, Spectrochimica Acta Part a-Molecular and Biomolecular Spectroscopy, 184 (2017) 211-219.
[28] A. Lemmerer, Covalent assistance to supramolecular synthesis: modifying the drug functionality of the antituberculosis API isoniazid in situ during co-crystallization with GRAS and API compounds, CrystEngComm, 14 (2012) 2465-2478.
[29] D.J. Shaw, K. Adamczyk, P. Frederix, N. Simpson, K. Robb, G.M. Greetham, M. Towrie, A.W. Parker, P.A. Hoskisson, N.T. Hunt, Multidimensional infrared spectroscopy reveals the vibrational and solvation dynamics of isoniazid, Journal of Chemical Physics, 142 (2015).
[30] A. Favila, M. Gallo, D. Glossman-Mitnik, CHIH-DFT determination of the molecular structure infrared spectra, UV spectra and chemical reactivity of three antitubercular compounds: Rifampicin, Isoniazid and Pyrazinamide, Journal of Molecular Modeling, 13 (2007) 505-518.
[31] A.k. Pandey, A. Bajpai, V. Baboo, A. Dwivedi, Structural, Electronic, and Vibrational Properties of Isoniazid and Its Derivative N-Cyclopentylidenepyridine-4-carbohydrazide: A Quantum Chemical Study, Journal of Theoretical Chemistry, 2014 (2014) 15.
[32] A.R. Owen, J.W. Golden, A.S. Price, W.A. Henry, W.K. Barker, D.A. Perry, Surface-Enhanced Vibrational Spectroscopy and Density Functional Theory Study of Isoniazid Layers Adsorbed on Silver Nanostructures, Journal of Physical Chemistry C, 118 (2014) 28959-28969.
[33] E. Akalin, S. Akyuz, Vibrational structure of free and hydrogen bonded complexes of isoniazid: FT-IR, FT-Raman and DFT study, Journal of Molecular Structure, 834 (2007) 492-497.
[34] A. Yilmaz, O. Bolukbasi, M. Bakiler, An experimental and theoretical vibrational spectra of isoniazide, Journal of Molecular Structure, 872 (2008) 182-189.
[35] A. Borba, A. Gomez-Zavaglia, R. Fausto, Molecular Structure, Infrared Spectra, and Photochemistry of Isoniazid under Cryogenic Conditions, Journal of Physical Chemistry A, 113 (2009) 9220-9230.
[36] S. Gunasekaran, E. Sailatha, S. Seshadri, S. Kumaresan, FTIR, FT Raman spectra and molecular structural confirmation of isoniazid, Indian Journal of Pure & Applied Physics, 47 (2009) 12-18.
[37] K.K. Hazarika, N.C. Baruah, R.C. Deka, Molecular structure and reactivity of antituberculosis drug molecules isoniazid, pyrazinamide, and 2-methylheptylisonicotinate: a density functional approach, Structural Chemistry, 20 (2009) 1079-1085.
[38] E. Gobinath, R.J. Xavier, Spectroscopic investigations, quantum chemical calculations, HOMO-LUMO and NBO/NLMO analysis of 4-pyridinecarbohydrazide, Spectrochimica Acta Part A-Molecular and Biomolecular Spectroscopy, 115 (2013) 815-822.
[39] K. Refson, P.R. Tulip, S.J. Clark, Variational density-functional perturbation theory for dielectrics and lattice dynamics, Physical Review B, 73 (2006).
[40] J.P. Perdew, K. Burke, M. Ernzerhof, Generalized gradient approximation made simple, Physical Review Letters, 77 (1996) 3865-3868.
[41] V. Milman, A. Perlov, K. Refson, S.J. Clark, J. Gavartin, B. Winkler, Structural, electronic and vibrational properties of tetragonal zirconia under pressure: a density functional theory study, Journal of Physics-Condensed Matter, 21 (2009).
[42] A.J. Ramirez-Cuesta, aCLIMAX 4.0.1, The new version of the software for analyzing and interpreting INS spectra, Computer Physics Communications, 157 (2004) 226-238.
[43] H.B.S. G.W.T. M. J. Frisch, G. E. Scuseria, , J.R.C. M. A. Robb, G. Scalmani, V. Barone, B. Mennucci, , H.N. G. A. Petersson, M. Caricato, X. Li, H. P. Hratchian, , J.B. A. F. Izmaylov, G. Zheng, J. L. Sonnenberg, M. Hada, , K.T. M. Ehara, R. Fukuda, J. Hasegawa, M. Ishida, T. Nakajima, , O.K. Y. Honda, H. Nakai, T. Vreven, J. A. Montgomery, Jr., , F.O. J. E. Peralta, M. Bearpark, J. J. Heyd, E. Brothers, , V.N.S. K. N. Kudin, R. Kobayashi, J. Normand, , A.R. K. Raghavachari, J. C. Burant, S. S. Iyengar, J.

Tomasi, , N.R. M. Cossi, J. M. Millam, M. Klene, J. E. Knox, J. B. Cross, , C.A. V. Bakken, J. Jaramillo, R. Gomperts, R. E. Stratmann, , A.J.A. O. Yazyev, R. Cammi, C. Pomelli, J. W. Ochterski, , K.M. R. L. Martin, V. G. Zakrzewski, G. A. Voth, , J.J.D. P. Salvador, S. Dapprich, A. D. Daniels, , J.B.F. O. Farkas, J. V. Ortiz, J. Cioslowski, , a.D.J. Fox, , Gaussian 09, Revision A.02, in: Gaussian 09, Revision A.02, Gaussian, Inc., Wallingford CT, 2009.
[44] A.M. Amado, J.C. Otero, M.P.M. Marques, L. de Carvalho, Spectroscopic and theoretical studies on solid 1,2-ethylenediamine dihydrochloride salt, ChemPhysChem, 5 (2004) 1837-1847.
[45] A.M. Amado, S.M. Fiuza, L. de Carvalho, P.J.A. Ribeiro-Claro, On the Relevance of Considering the Intermolecular Interactions on the Prediction of the Vibrational Spectra of Isopropylamine, Journal of Chemistry, (2013).
[46] A.M. Amado, C. Azevedo, P.J.A. Ribeiro-Claro, Conformational and vibrational reassessment of solid paracetamol, Spectrochimica Acta Part A-Molecular and Biomolecular Spectroscopy, 183 (2017) 431-438.
[47] J.P. Merrick, D. Moran, L. Radom, An evaluation of harmonic vibrational frequency scale factors, Journal of Physical Chemistry A, 111 (2007) 11683-11700.
[48] M.C. Costa, M. Sardo, M.P. Rolemberg, J.A.P. Coutinho, A.J.A. Meirelles, P. Ribeiro-Claro, M.A. Krahenbuhl, The solid-liquid phase diagrams of binary mixtures of consecutive, even saturated fatty acids, Chemistry and Physics of Lipids, 160 (2009) 85-97.
[49] N.F.C. Mendes, M.M. Nolasco, P.J.A. Ribeiro-Claro, Effects of hydrogen-bond and cooperativity in the vibrational spectra of Luminol, Vibrational Spectroscopy, 64 (2013) 119-125.
[50] A.E.R. E. D. Glendening, J. E. Carpenter, and F. Weinhold, NBO Version 3.1.
[51] L.H. Jensen, The crystal structure of isonicotinic acid hydrazide, Journal of the American Chemical Society, 76 (1954) 4663-4667.
[52] T.N. Bhat, T.P. Singh, M. Vijayan, Isonicotinic-acid hydrazide - reinvestigation, Acta Crystallographica Section B-Structural Science, 30 (1974) 2921-2922.
[53] M.C. Shivaglal, S. Singh, Effect of hydrogen-bonding and cooperativity on the stretching force-constants of formamide., International Journal of Quantum Chemistry, 44 (1992) 679-690.
[54] R.D. Parra, S. Bulusu, X.C. Zeng, Cooperative effects in one-dimensional chains of three-center hydrogen bonding interactions, Journal of Chemical Physics, 118 (2003) 3499-3509.
[55] T.M. Silva, S.M. Fiuza, M.P.M. Marques, L. de Carvalho, A.M. Amado, Conformational study and reassessment of the vibrational assignments for Norspermidine, Spectrochimica Acta Part A-Molecular and Biomolecular Spectroscopy, 157 (2016) 227-237.
[56] M. Boczar, R. Kurczab, M.J. Wojcik, Theoretical and spectroscopic studies of vibrational spectra of hydrogen bonds in molecular crystal of beta-oxalic acid, Vibrational Spectroscopy, 52 (2010) 39-47.
[57] N. Rekik, B. Oujia, M.J. Wojcik, Theoretical infrared spectral density of H-bonds in liquid and gas phases: Anharmonicities and dampings effects, Chemical Physics, 352 (2008) 65-76.
[58] N. Rekik, Signature of Congregated Effects of Mechanical and Electrical Anharmonicities, Fermi Resonances, and Dampings on the IR Spectra of Hydrogen Bonded Systems: Quantum Dynamic Study, Journal of Physical Chemistry A, 121 (2017) 3555-3566.
[59] N.B. Colthup, L.H. Daly, S.E. Wiberley, Chapter 9 - Carbonyl Compounds, in: Introduction to Infrared and Raman Spectroscopy (Second Edition), Academic Press, 1975, pp. 306., in.
[60] F. Zhang, H.W. Wang, K. Tominaga, M. Hayashi, Mixing of intermolecular and intramolecular vibrations in optical phonon modes: terahertz spectroscopy and solid-state density functional theory, Wiley Interdisciplinary Reviews-Computational Molecular Science, 6 (2016) 386-409.

Figure Captions

Scheme 1 – Representation of Isoniazid, with the atom labelling used throughout the text.

Figure 1 – Optimized geometry of the isolated molecule (Gaussian09, left) and the crystalline structure (CASTEP, right). Torsional angles for the isolated molecule and relevant intermolecular contacts in the crystalline structure are shown (see text).

Figure 2 – Representation of the displacement vectors associated with the out-of-plane ring mode at 804 cm^{-1} and the nearly in-plane mode at 1190 cm^{-1}. For better readability, displacement vectors of hydrogen atoms are scaled to 50%.

Figure 3 – INS (a), Raman (b), and infrared (ATR, c) spectra of isoniazid, compared with the infrared spectrum of N-deuterated isoniazid (isoniazid-d_3, d) and the calculated infrared spectrum (CASTEP, e), including the visualization of atomic displacement vectors for the normal modes corresponding to the higher wavenumber band (right) and the two lower wavenumber bands (left). The asterisks (in line d) mark the bands from residual non-deuterated form. For the sake of clarity, the calculated bands at ca. 3000 cm^{-1}, assigned to νN_2H_2 stretching modes, have been cut at about 5% of their intensity.

Figure 4 – Experimental (a) and calculated (CASTEP, b) inelastic neutron scattering spectra of isoniazid. The dashed arrow indicate the ill-calculated frequency (see text).

Figure 5 – Experimental (a) and calculated (CASTEP, b) infrared spectra of isoniazid. The dashed arrows indicate the ill-calculated frequencies (see text).

Figure 6 – Experimental far-infrared spectrum (a) and inelastic neutron scattering spectrum (b) of isoniazid, compared with their calculated (colored) versions, using the PBE functional.

Figure 7 - Representation of the displacement vectors associated with the libration mode at 129 cm^{-1}. The rotation of the molecules stretches the hydrogen bond contacts not only between the molecular pair show (dashed line), but also between the molecules above and below (pointed lines).

Table 1 – Selected geometrical parameters of isoniazid.

Parameter	X-ray [28]	CASTEP (fixed cell)	CASTEP (fully opt)	Gaussian
Cell lengths/A				
a	3.78	3.78[a)]	4.7063	-
b	11.29	11.29[a)]	11.336	-
c	14.68	14.68[a)]	14.68	-
Bond lengths/pm				
C6=O	122.2	124.1	124.4	122.2
C6-N2	134.5	136.1	136.3	136.5
N2-N3	142.2	143.8	144.1	139.9
Bond angles/º				
C1-C6-O	122.2	121.8	121.4	122.4
C1-C6-N2	115.3	115.8	116.7	115.7
C6-N2-N3	120.4	119.4	118.7	120.2
Dihedral angles				
C2C1-C6O (θ1)	-17.9	-19.1	-24.6	-24.8
OC6-N2N3 (θ2)	-5.5	-7.7	-5.3	6.1
C6N2-N3Ha (θ3)	-25.5	-18.4	-10.9	-78.6
Intermolecular/pm				
N2(-H)…N3	291.5	288.1	296.8	297 [b)]
N3(-H)…N1	304	295.7	304.2	307 [b)]
C2(-H)…O	325.2	328.4	338.8	348.6 [b)]
π-π (C1…C1') [c)]	378.7	378.7	407.6	383.9 [b)]

a) Fixed values; b) Values from molecular pairs; c) Distance between C1 atoms of the π-staking molecules.

Table 2 - Observed (FT-IR, Raman, and INS) and calculated (CASTEP) wavenumbers of isoniazid in the solid state (wavenumbers/cm^{-1})

Experimental			Calculated	Aproximate description	
ATR-FTIR	**FT-Raman**	**INS**	**CASTEP** [a)]	**Pyr ring**	**Carbohydrazide**
3303	3302		3283		**ν N3Ha**
3105	3107		3063*IR		**νs N_2H_2**
(3050)[b]	(3050)[b]		3028*IR		**νas N_2H_2**
3094	3091	3097	3130	**νCH (20a)**	
3069	3065	-	3109	**νCH (20b)**	
3054	3052	-	3088	**νCH (2)**	
-	3026	-	3071	**νCH (7b)**	
1661	1668	-	1590*IR		**ν C=O**
1632	1641	1633	1643		**NH_2 scissor**
1603	1601	-	1580 IR	**ν ring (8a)**	
1552	1550	1564	1553		**β NH**
1535	-	-	*1530*	**ν ring (8b)**	
1490	1492	1496	1472	**ν ring (19a)**	
1409	1410	1412	1396	**ν ring (19b)**	
1332	1332	1346	1331		**NH_2 twist**
-	-	1324	1307	**βCH (3)**	
1321	1320	-	*1296*	**ν C1-C6 (13)**	
1263	1266	1266	1250	**ν ring (14)**	
1219	1217	1220	1203	**β CH (9a)**	
1193	1186	1195	1190		**ν N(2)-N(3)**
1141	1130	1140	1128		**ν C(6)-N(2)**
1098	1094	1095	1081	**β CH (15)**	
1063	1056	1057	1047	**β CH (18a)**	
-	1002	-	991	**α ring (12)**	
-	-	998	988	**γ CH (5)**	
994	993	-	*980*	**ν ring (1)**	
963	964	967	957	**γ CH (17a)**	
886	886	-	881		**γ NH**
-	-	891	876	**γ CH (10a)**	
846	848	852	847		**NH_2 wagg**
-	-	786	804	**γ CH (17b)**	
742	-	749	739	**δ ring (4)**	
	681	682	674	**α ring (6a)**	
671	-	-	*672*		**γ C=O**
658	665	663	654	**α ring (6b)**	
503	503	507	516		**βC1C6N2**

438	434	439	416	**δ ring (16b)**	
397	397	422	478*		**τ NH2**
380	372	381	373	**δ ring (16a)**	
354	362	366	350		**βC6N2N3**
336	336	340	*331*		**β C=O**
324	326	332	318		
261		266	273		**τ C6-N2** [c]
246	252	256	256		
229		229	207	**β ring-R (18b)**	
213	220	221	202		
	178	176	175	**γ ring-R (11)**	
156	157	166	153		
		138	133	**τ C1-C5**	
123			130		

a) Maxima of the INS simulated spectrum, except when otherwise indicated (IR= infrared simulated spectrum); Wavenumbers marked with asterisk are considered ill-calculated (see text); b) Estimated from isotopic shifts; c) nominally torsion around C6–N2, but better described as out-of-plane N2–NH_2 deformation (γN2–NH_2).

Table 3 - *Observed (FT-IR, Raman, and INS) and calculated (CASTEP) wavenumbers of isoniazid in the solid state (wavenumbers/cm^{-1}).*

Experimental			Calculated	
ATR/FTIR	**Raman**	**INS**	**CASTEP** [a)]	**Mode description** [b)]
		129	128	Libration (Ic) , with N2-H…N3 stretching
113			118 IR	Libration Ia (mainly Hydrazine torsion)
		110	110	Libration-translation, with N3-H…N1 stretching
	96	101	95	Libration Ia (mainly Pyridyl torsion)
91		89	100	Libration (butterfly type)
80	83	80	80	Translation (along c), with C-H…O stretching
67		69	68	Libration Ia (mainly Pyridyl torsion)
57		57	58	Libration Ia (mainly Pyr torsion)
		47	42	Libration Ia (mainly Pyr torsion)
		37	32	Translation (along a), Libration Ia

a) Maxima of the INS simulated spectrum, except when otherwise indicated (IR= infrared simulated spectrum); b) Crystallographic cell axes as shown in Fig.1; Molecular inertia axes: Ia is slightly deviated from the C1-C6 direction, Ic is nearly perpendicular to the ring plane.

Highlights

Discrete and periodic DFT calculation for isoniazid crystal are performed.

The normal modes are fully described and previous misassignments are corrected

The unusual combination of NH oscillators in the NH stretching region is discussed
Factor group splitting for large amplitude molecular vibrations is reported

Full assignment from a blend of spectroscopic and computational methods

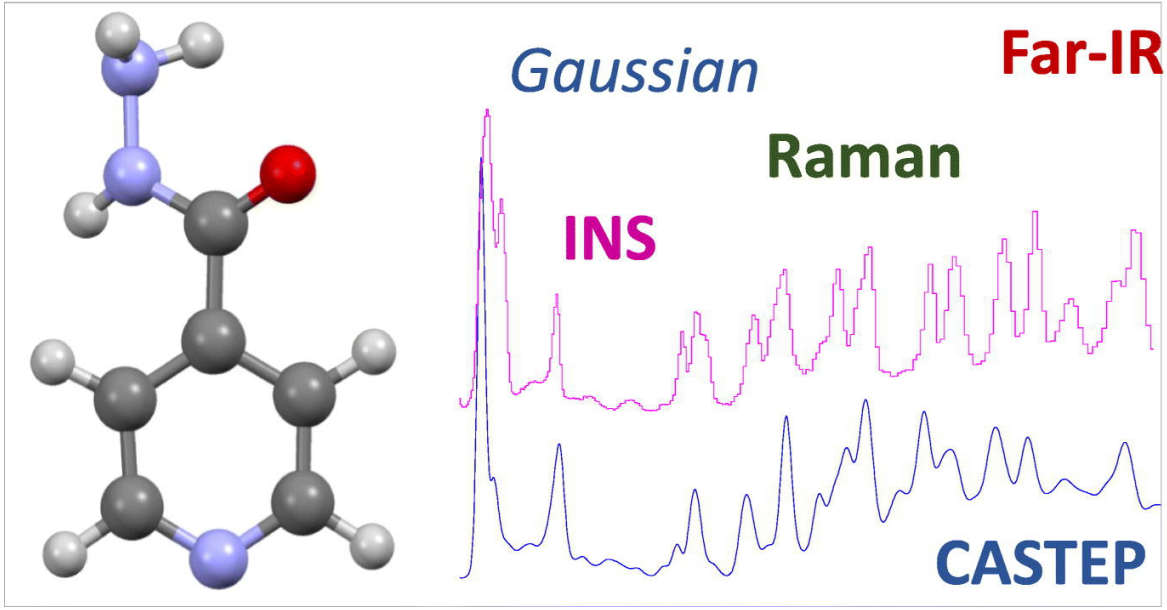

P.J.A. Ribeiro-Claro, P.D. Vaz, M.M. Nolasco and A.M. Amado

Understanding the Vibrational Spectra of Crystalline Isoniazid: Raman, IR and INS Spectroscopy and Solid-State DFT Study

Graphics Abstract

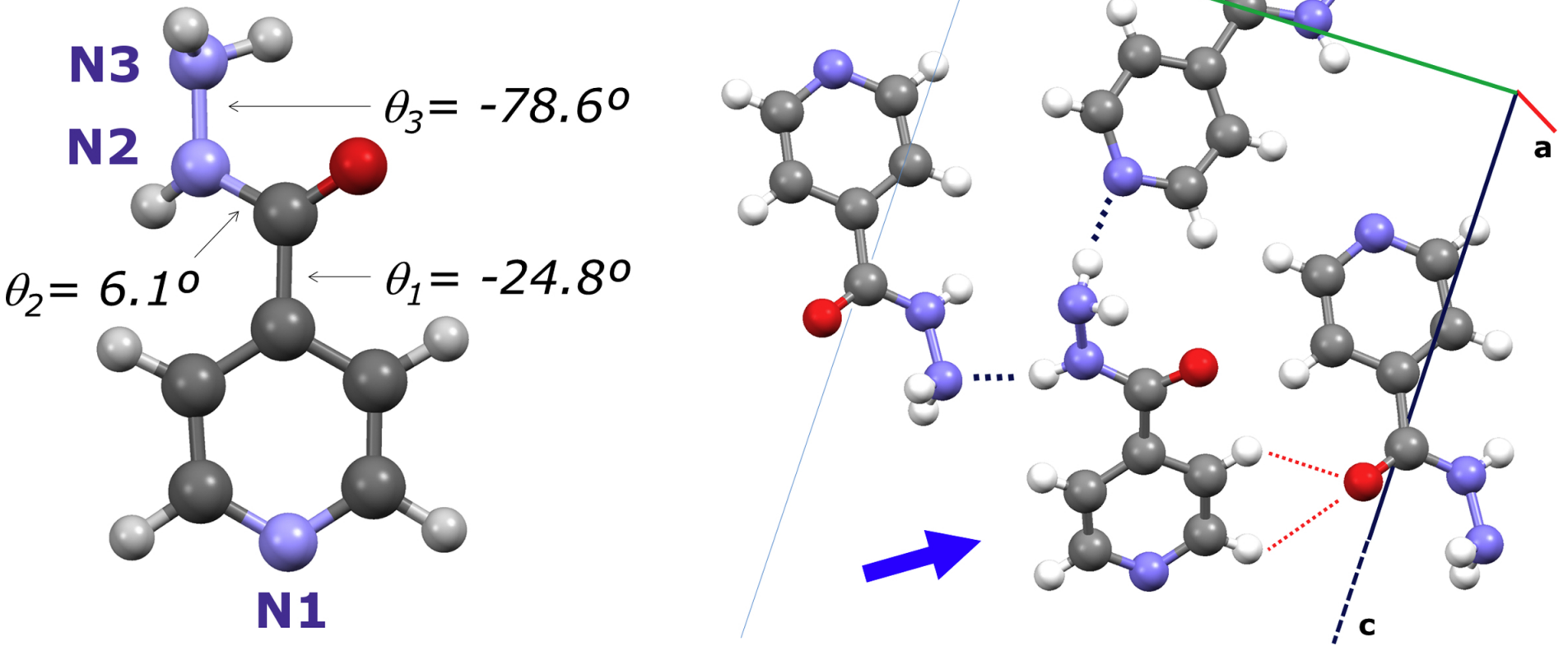

Figure 1

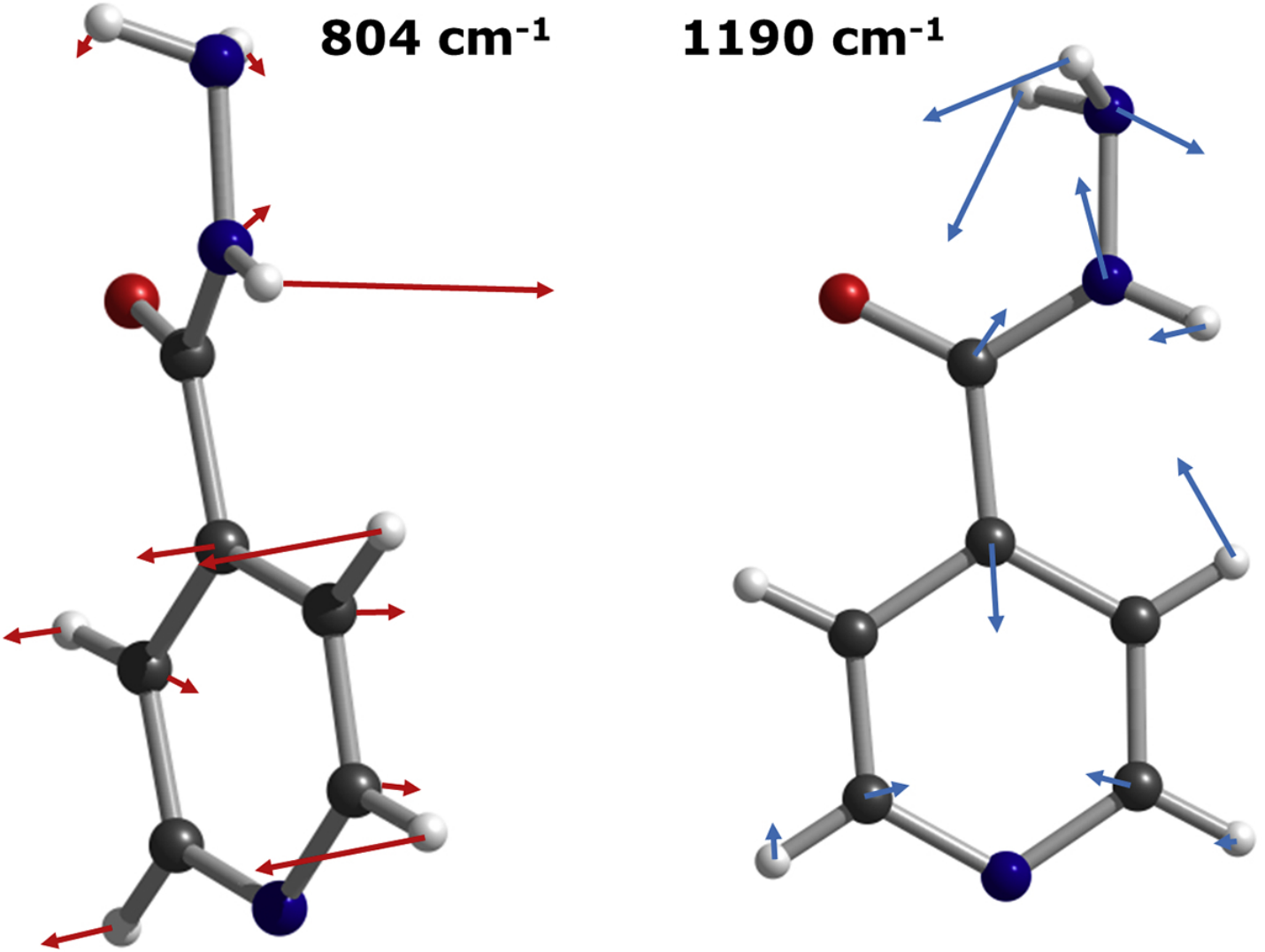

Figure 2

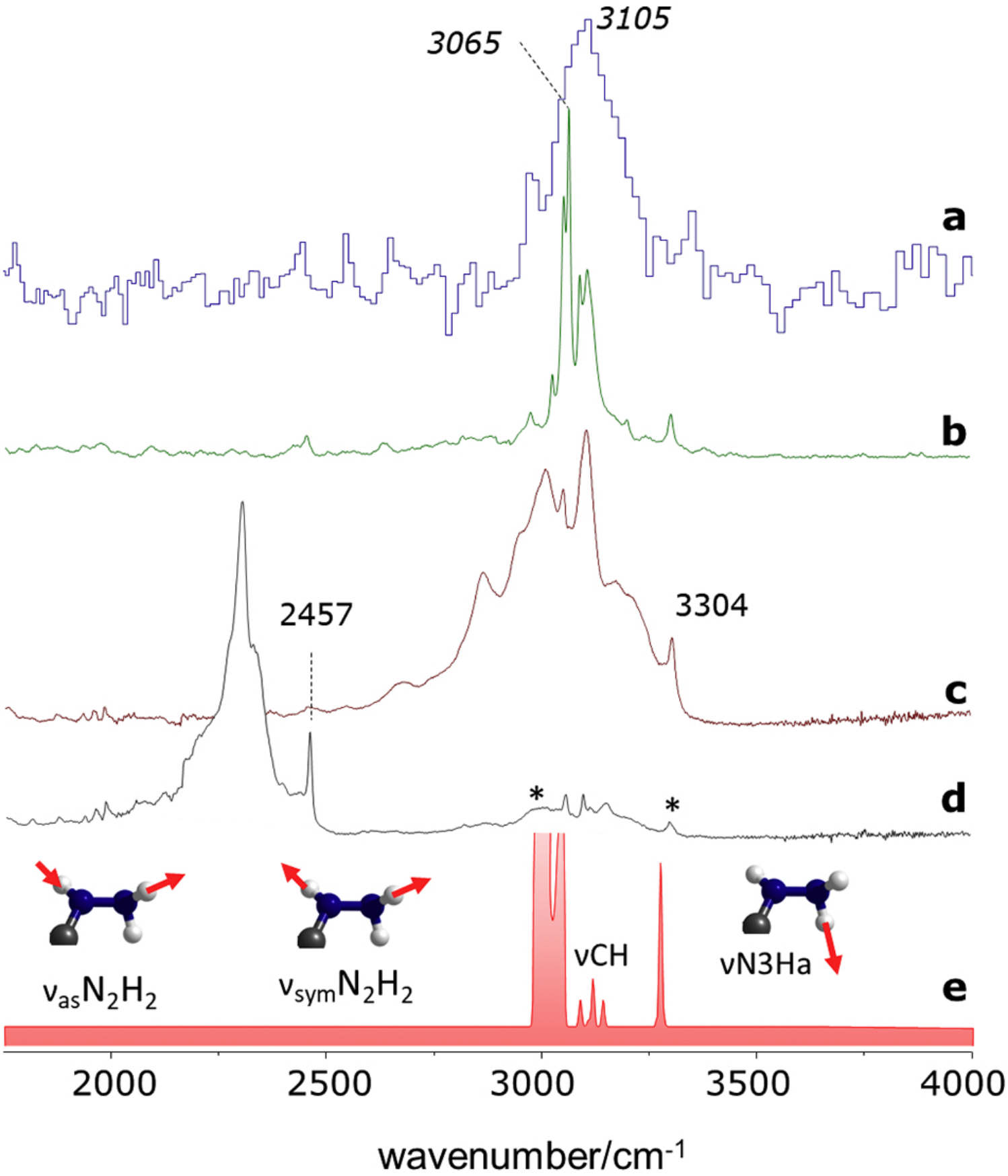
3105
3065
a
b
2457
3304
c
d
*
*
vCH
vN3Ha
e
$\nu_{as}N_2H_2$
$\nu_{sym}N_2H_2$
2000
2500
3000
3500
4000
wavenumber/cm^{-1}

Figure 3

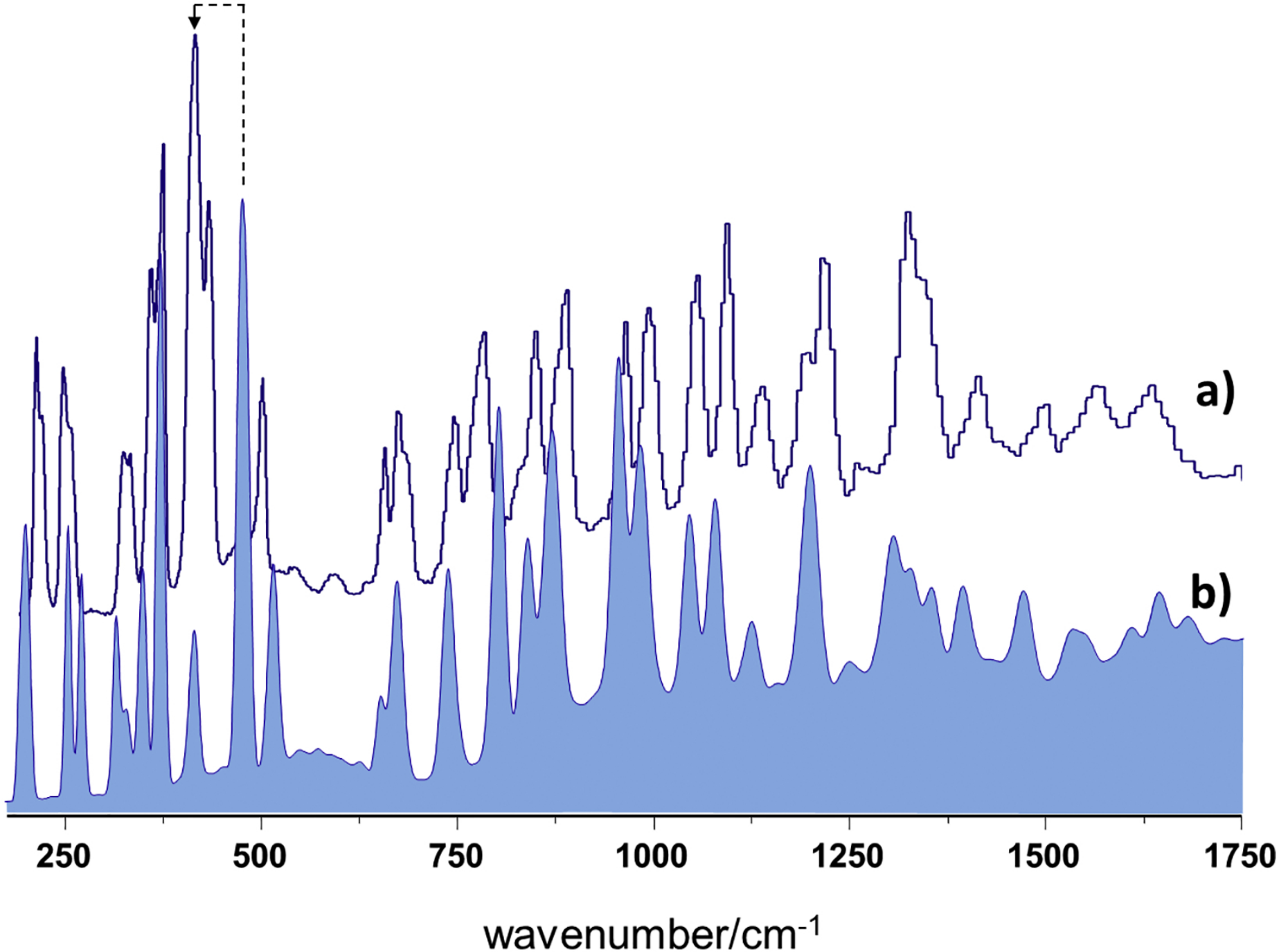

Figure 4

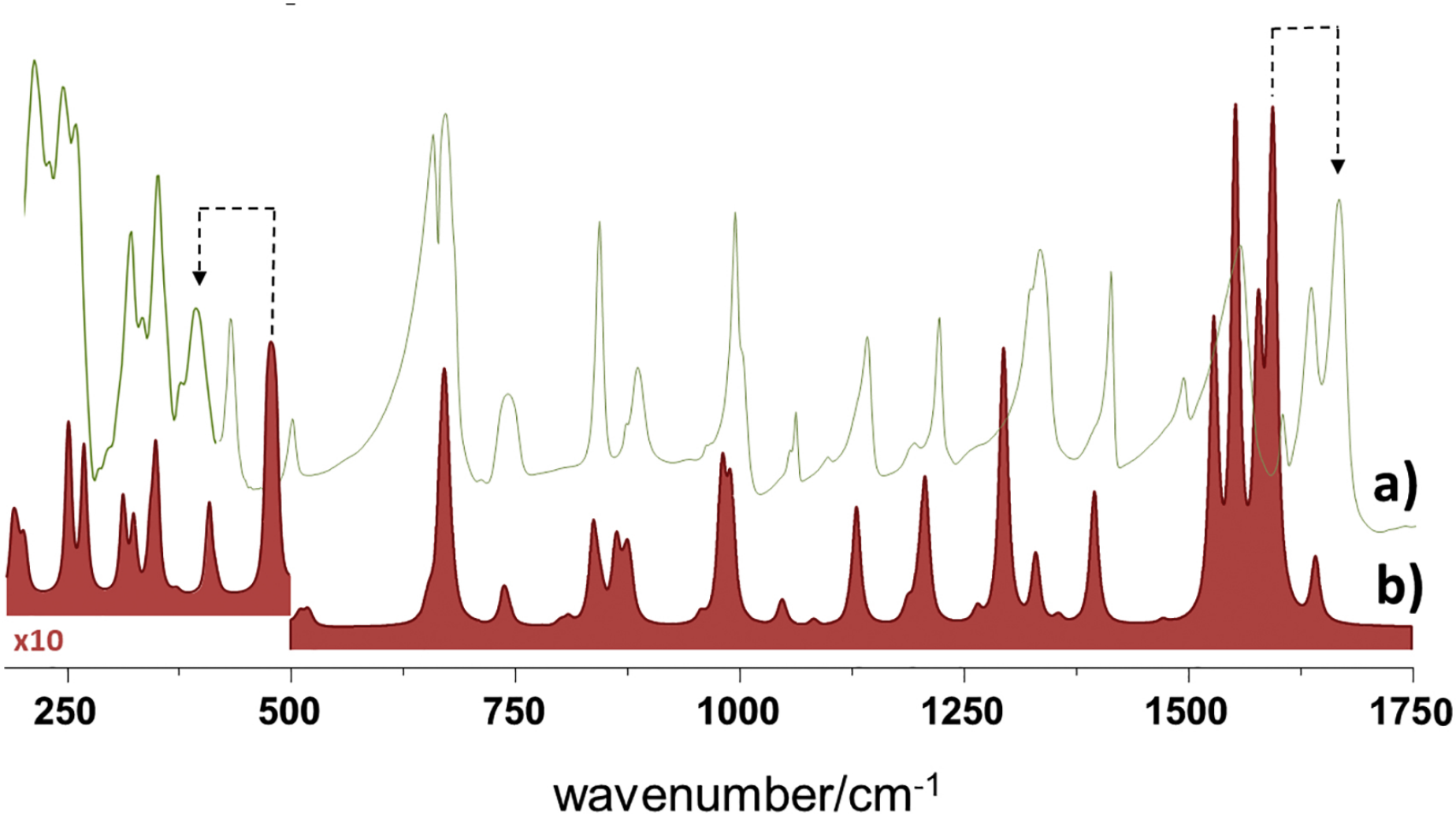

Figure 5

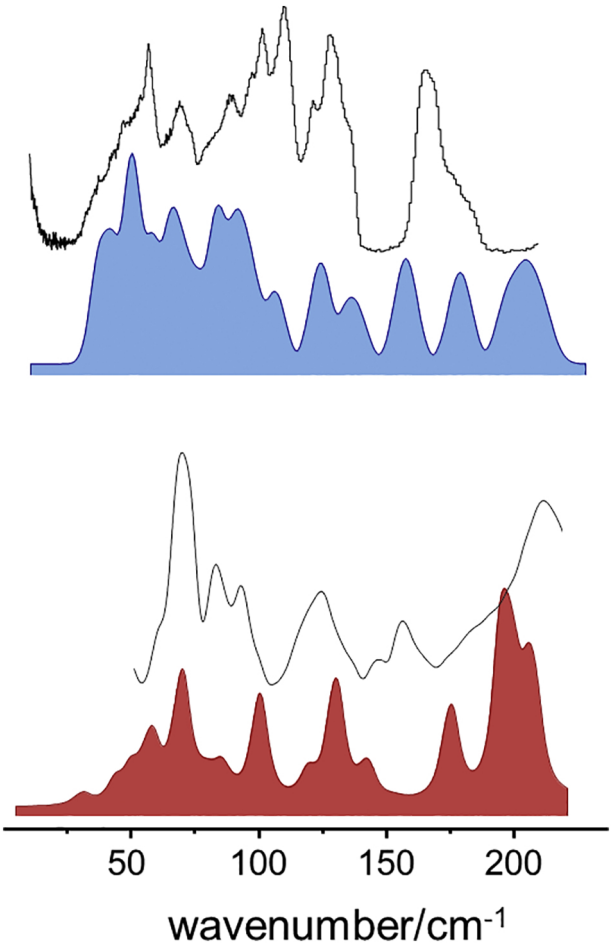

Figure 6

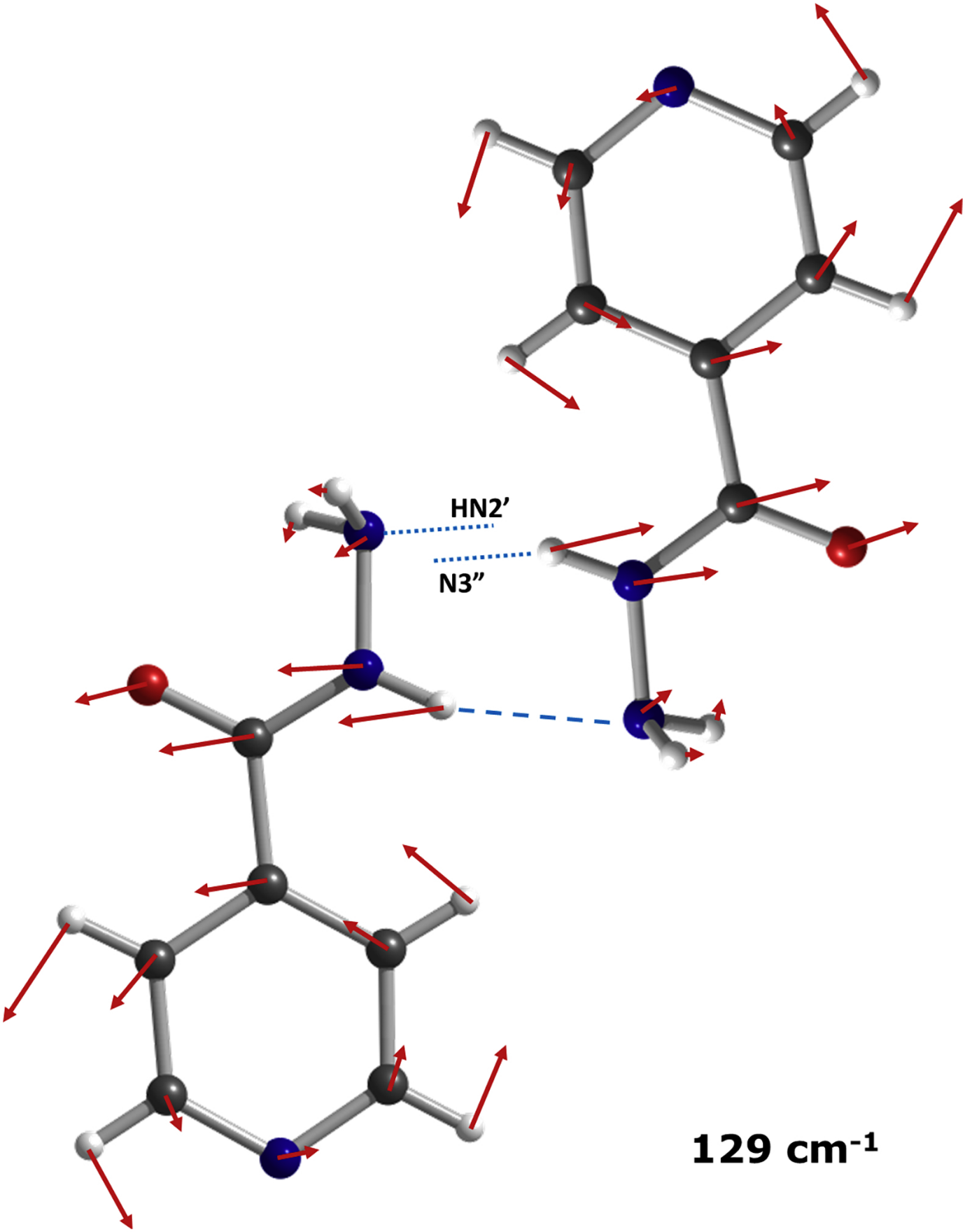

Figure 7